Downloaded from http://sp.lyellcollection.org/ by guest on April 28, 2017

Structural and petrophysical effects of overthrusting on highly porous sandstones: the Aztec Sandstone in the Buffington window, SE Nevada, USA

LUISA F. ZULUAGA[1,2], HAAKON FOSSEN[1,3,4]*, GREGORY BALLAS[5,6] & ATLE ROTEVATN[1]

[1]*Department of Earth Science, University of Bergen, Allégaten 41, 5007 Bergen, Norway*

[2]*Centre for Integrated Petroleum Research (Uni Research CIPR), Allégaten 41, 5007 Bergen, Norway*

[3]*University Museum of Bergen – The Natural History Collections, University of Bergen, PO Box 7800, 5020 Bergen, Norway*

[4]*Instituto de Geociências, Universidade de São Paulo, Rua do Lago, 562, Cidade Universitária, São Paulo-SP CEP 05508-080, Brazil*

[5]*Institut Français de Recherche pour l'Exploitation de la Mer, Pointe du Diable, 29280 Plouzané, France*

[6]*Geosciences Montpellier, Université de Montpellier, Campus Triolet, CC060, Place Eugène, Bataillon, 34095 Montpellier Cedex 05, France*

**Correspondence: haakon.fossen@uib.no*

Abstract: Little is known about the effect of thrusting on lithological and petrophysical properties of reservoir sandstone. Here we use field observations, probe permeability measurements and thin-section analysis along ten transects from the Muddy Mountain thrust contact downwards into the underlying Jurassic Aztec Sandstone to evaluate the nature and extent of petrophysical and microstructural changes caused by the thrusting. The results reveal a decimetre- to metre-thick low-permeable (≤50 mD) and indurated (0–3% porosity) zone immediately beneath the thrust contact in which dominant microscale processes, in decreasing order of importance, are (1) cataclasis with local fault gouge formation; (2) pressure solution; and (3) very limited cementation. From this narrow zone the petrophysical and microstructural effect of the thrusting decreases gradually downwards into a friable, highly porous (*c.* 25%) and permeable (≤2 D) sandstone some 50–150 m below the thrust, in which strain is localized into deformation band populations. In general, the petrophysical properties of the sandstone as a result of overthrusting reveal little impact in overall primary reservoir quality below some tens of metres into the footwall, except for the relatively minor baffling effect of deformation bands.

Our understanding of how porous sandstones respond to tectonic deformation largely relate to the extensional tectonic regime, where normal faults form through a history of deformation band formation and clustering (e.g. Aydin & Johnson 1983; Shipton & Cowie 2001; Fossen & Bale 2007; Schueller *et al.* 2013), or to fault-propagation folds in the contraction regime where deformation is distributed within an upwards-widening zone of strain (Brandenburg *et al.* 2012; Zuluaga *et al.* 2014). In contrast, little is known about the structural and petrophysical effects of overthrusting on sandstone reservoirs. An example of such a setting is the Muddy Mountain thrust in SE Nevada (Longwell 1922), which developed during the Late Cretaceous Sevier orogeny, and has been referred to as an erosional thrust that moved subhorizontally and probably at very shallow depths, emplacing an extensive thrust nappe of middle Cambrian carbonates and younger rocks over highly porous Jurassic sandstone (Johnson 1981; Price & Johnson 1982).

The erosional level in the Buffington tectonic window in SE Nevada allows us to assess the deformation from the thrust and several hundred metres vertically into the underlying aeolian Jurassic Aztec Sandstone. Large portions of this sandstone, which are very well exposed within the window (Figs 1 & 2a), have preserved remarkably good

From: Ashton, M., Dee, S. J. & Wennberg, O. P. (eds) *Subseismic-Scale Reservoir Deformation*. Geological Society, London, Special Publications, **459**, https://doi.org/10.1144/SP459.8
© 2017 The Author(s). Published by The Geological Society of London. All rights reserved.
For permissions: http://www.geolsoc.org.uk/permissions. Publishing disclaimer: www.geolsoc.org.uk/pub_ethics

Downloaded from http://sp.lyellcollection.org/ by guest on April 28, 2017

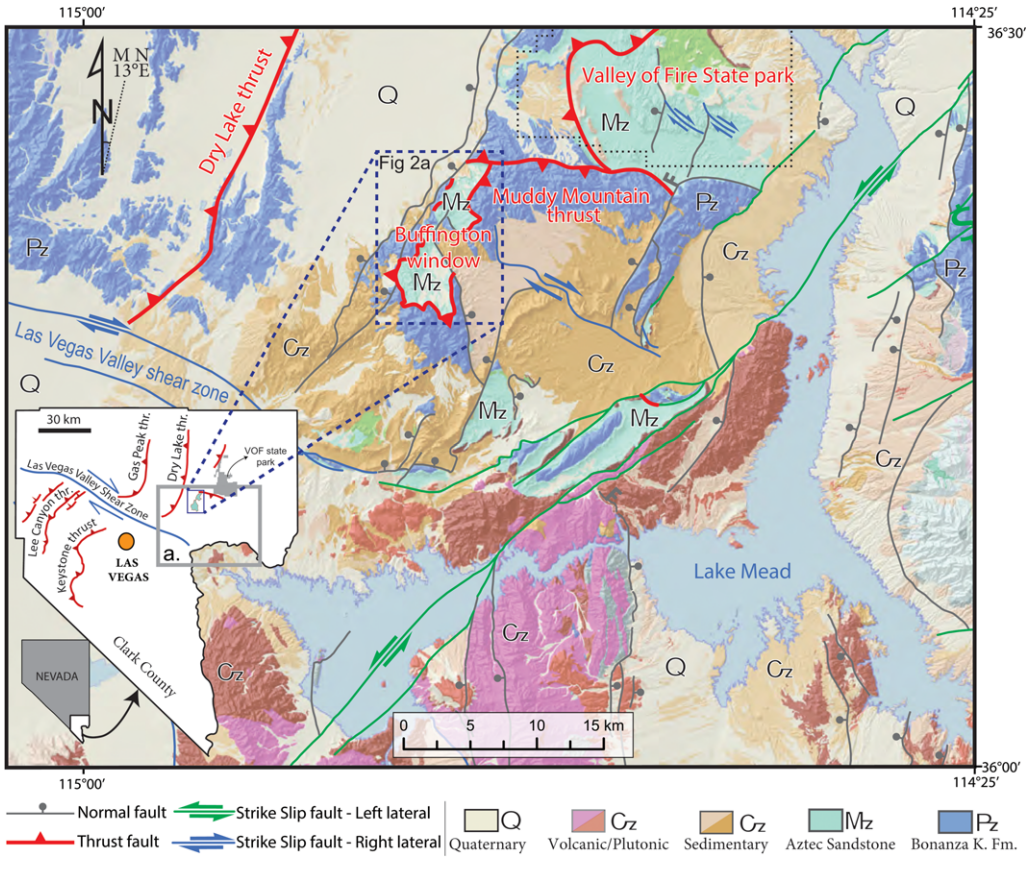

Fig. 1. Geological map of the study area in Nevada. Bottom left: location of the study area in Clark county, SE Nevada, with major thrust and strike-slip tectonic features shown. Q: Quaternary; Cz: Cenozoic; Mz: Mesozoic; Pz: Palaeozoic.

overall petrophysical properties, in spite of the fact that it was overridden by an extensive (800 km^2; Beard *et al.* 2007) thrust sheet of >2 km (Willemin 1984) or 4–5 km (Brock & Engelder 1977) thickness that moved at least 40 km to the ESE (Price & Johnson 1982). However, the tectonic deformation of the footwall sandstone in the Buffington window increases towards the thrust, as demonstrated by Brock & Engelder (1977) based on three traverses into the footwall. They reported intense deformation and cataclasis along the thrust contact, where the sandstone is very compacted and indurated, as well as the transition to the much less strained sandstone up to 75 m into the footwall. Below this zone more recent work by Fossen *et al.* (2015) shows that distributed populations of deformation bands occur in Aztec Sandstone of good reservoir quality (permeability $\leq$ 2 Darcy, porosity *c.* 20%, this study), for which types and orientations of deformation bands are discussed in terms of the stress history of the Muddy Mountain thrust movement and the stress field of the Sevier orogeny.

In this contribution we re-examine the microstructural effect of overthrusting on the Aztec Sandstone, together with permeability and porosity observations along 10 transects from the thrust and 50–150 m downwards into the sandstone. The ultimate aim was to quantify petrophysical properties of footwalls of shallow overthrusts involving porous rocks, with applicability for exploration and reservoir management in areas of contractional deformation where relatively large-scale overthrusting is involved.

Tectonic framework

General setting

The Buffington tectonic window is located *c.* 45 km NE of Las Vegas and 6 km west of Valley of Fire

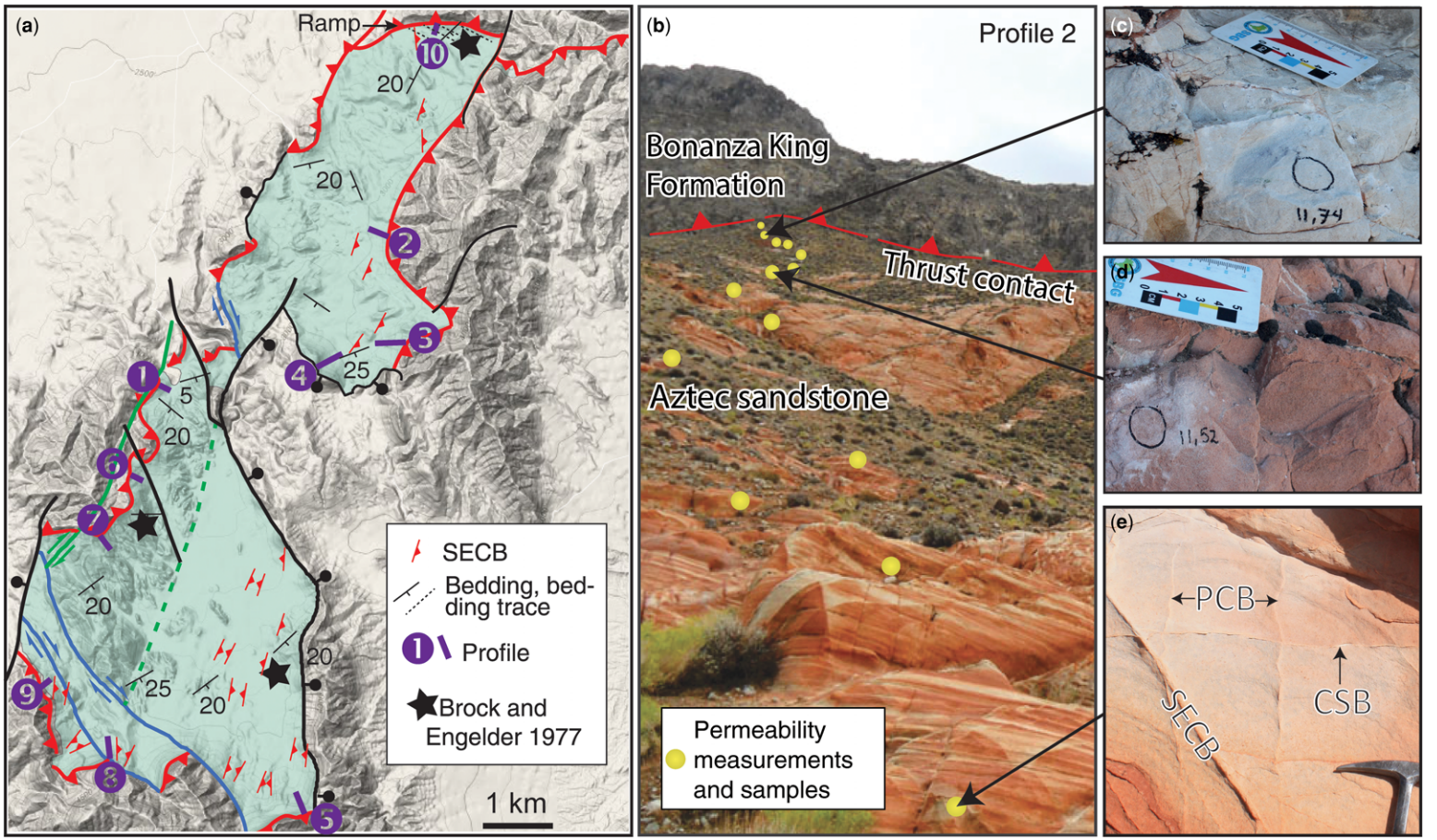

Fig. 2. (**a**) Map of the Buffington tectonic window (Aztec Sandstone in transparent green shade) showing locations of our ten profiles. (**b–e**) Example of permeability profiling procedure: measurements made from the thrust contact downwards, after exposing fresh rock surfaces. Notice differences in sandstone appearance: near the thrust (c), and furthest from the thrust (e). Deformation bands, pure compaction bands (PCB) and shear-enhanced compaction bands (SECB) are characteristic of the most porous layers (e). Cataclastic shear bands (CSB) are found in highly porous and non-porous zones.

Downloaded from http://sp.lyellcollection.org/ by guest on April 28, 2017

Downloaded from http://sp.lyellcollection.org/ by guest on April 28, 2017

State Park, in Clark County of SE Nevada, USA (Fig. 1). The window is a *c.* 28 km^2 exposure of the Lower Jurassic Aztec Sandstone underneath the Muddy Mountain thrust (Fig. 2a), which forms part of an imbricate thrust system with ESE transport direction (Longwell 1922; Bohannon 1983; Carpenter & Carpenter 1994; DeCelles & Coogan 2006). The Sevier-age system was subsequently affected by middle Miocene extensional Basin and Range tectonism that caused block translation and rotation, as well as far-reaching erosion of the nappe complex (Wernicke *et al.* 1988; Langenheim *et al.* 2001). Subsequently, the thrust system was offset in a right-lateral sense by the Las Vegas Valley Shear Zone during early Pliocene times; at present, the southern continuation of the Muddy Mountain thrust is correlated in the SW with the Keystone thrust (Price & Johnson 1982). Normal faults affect the thrust system and the thrust is at least locally reactivated in extension, although this may be difficult to recognize or quantify in the field.

Stratigraphy

The Aztec Sandstone (Figs 2 & 3) is a fine- to coarse-grained (100–400 μm; Fig. 4) cross-bedded quartz-arenite, weakly cemented by hematite (Longwell *et al.* 1965) and deposited in a vast erg setting during Early Jurassic times (Marzolf 1990). The unit correlates to the Navajo and Nugget sandstones in the Colorado Plateau (Blakey *et al.* 1988). Aeolian cross-beds and bounding surfaces are well preserved, and the Aztec Sandstone exhibits permeability values of several Darcy and porosities up to 25% in the least-deformed and best-sorted layers (this study). In general the beds are rotated, mostly to the SE in the southern part of the window, but the overall variation in orientation of bedding (Fig. 2a) suggests that the sandstone was gently folded during thrusting. The present orientations of the bedding and the thrust contact are, however, influenced by steeper Basin and Range extensional faults.

In terms of composition, the bulk mineralogy of the samples analysed with a scanning electron microscope with backscattered electrons (SEM-BSE) and X-ray spectroscopy show that the grain framework is composed almost entirely of quartz ($\geq$95%), with a small component of feldspars (3 ± 2%) and traces of clay minerals (illite and kaolinite) (Figs 3 & 5). In some of the samples from the most porous parts of the sandstone, goethite and hematite grain coatings are present, providing weak cements in the friable varieties of the Aztec Sandstone (Fig. 3f). A lack of quartz/calcareous cement except for very sporadic grain overgrowths are also characteristic in these friable parts, whereas in some samples closer to the thrust contact, secondary vein fillings and matrix of calcareous composition was found.

In the study area, the Muddy Mountain thrust places a highly brecciated dolomitic interval on top of the Jurassic Aztec Sandstone, namely the middle Cambrian Bonanza King Formation, which was deposited in cyclic shallow-marine to shelf environments (Montañez & Osleger 1996). An unnamed siliciclastic unit is locally found between the Aztec Sandstone and the dolomitic Bonanza King Formation, spatially restricted to the middle-western sector of the Buffington window (Fig. 3a). This unnamed unit has been interpreted as molassic and fluvial sediments, representing erosional products derived from the toe of the advancing nappe during its emplacement (Brock & Engelder 1977; Johnson 1981). In the Keystone thrust area, this unit has been informally named the Lavinia wash sequence (Carr 1980).

This interpretation is based on the character of the unit which, in terms of grain framework and sedimentary structures, differs from those of the Aztec Sandstone being texturally and compositionally more immature. The molasse consists of fine-grained and very poorly sorted sandstone with local calcareous matrix (Fig. 3e), and the channels contain conglomeratic clasts of carbonates and sandstones in siliciclastic/calcareous matrix (Fig. 3c). In addition, these units crop out with a gentler topographic expression, in contrast to the weathering-resistant and fractured Aztec Sandstone (Fig. 3a).

Thrust contact and adjacent footwall sandstone

Below the Muddy Mountain thrust and the molassic intervals, the Aztec Sandstone in the Buffington window crops out in essentially two manners: as an indurated and intensively macro-fractured sandstone resistant to weathering (Fig. 3a), spatially restricted to the western part of the window; and a more friable sandstone elsewhere (Fig. 3d), in which the terrain is generally flat and more extensively covered by quaternary sediments with scattered mounds of sandstone, especially in the southeastern and northern parts of the window (see rugged terrain of the western part of the window v. the comparatively flat terrain in Fig. 2a). In all cases, the sandstone becomes increasingly cohesive towards the thrust contact.

The thrust nappe rests directly on the Aztec Sandstone (Fig. 3d) with a variably developed fault gouge (Fig. 3b), except for the southwestern contact where the footwall and hanging wall are separated by molasse sediments (Fig. 3a) or fluvial channels (Fig. 3c). In the northern part of the window (at Profile 10 in Fig. 2) the thrust cuts upsection

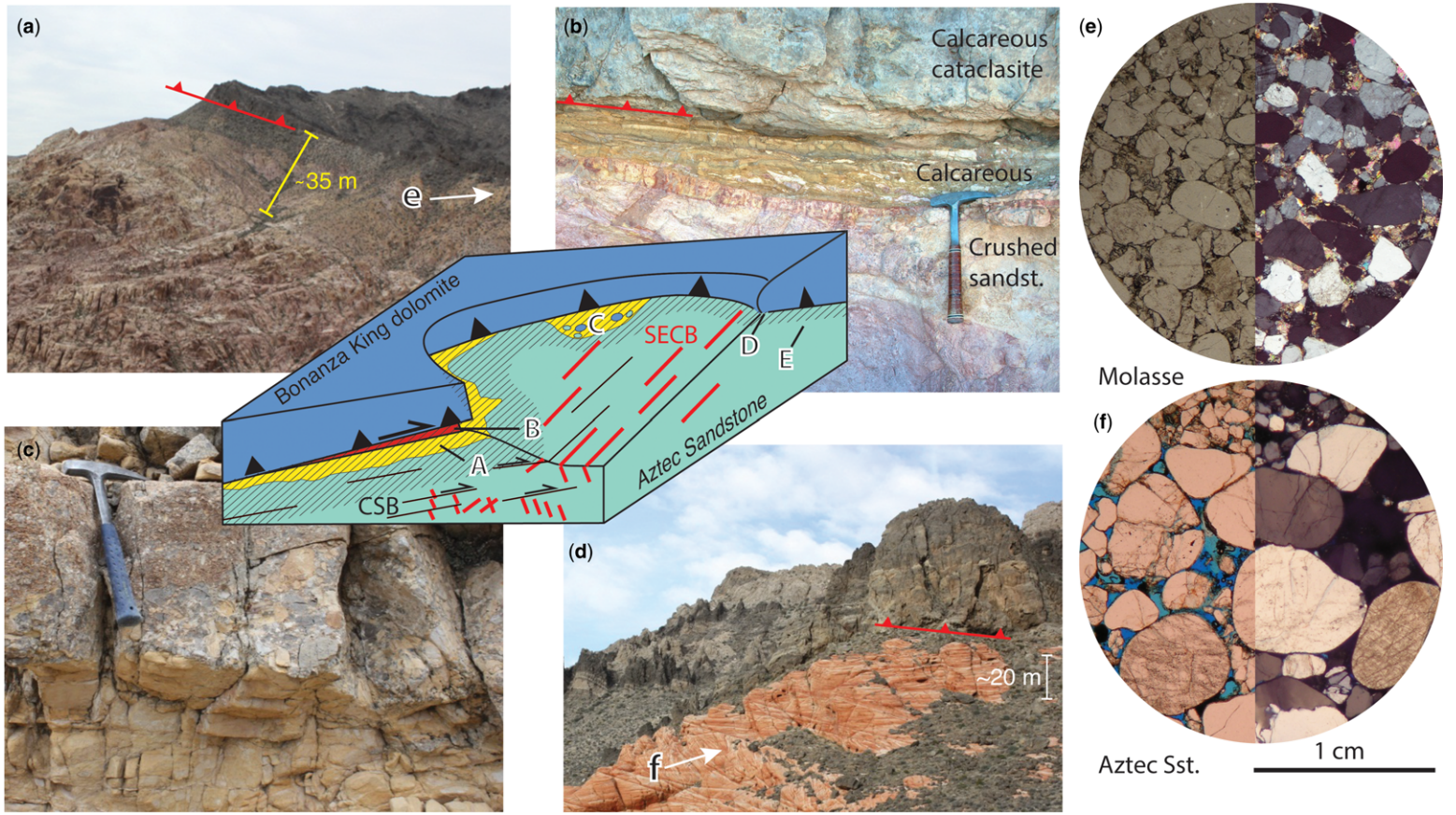

Fig. 3. Nature of the thrust contact at different places in the Buffington tectonic window: diagrammatic sketch in the middle and corresponding photo examples. (**a**) Decametre-thick interval of molassic sediments (thickness highlighted in yellow is *c.* 35 m) that at outcrop scale can be distinguished from the Aztec Sandstone by its fluvial character (lack of eolian crossbedding) (near profiles 7 and 6). (**b**) Fault gouge at the thrust contact, composed of crushed sandstone overlain by a calcareous foliated cataclasite. (**c**) Fluvial channel fills with rounded clasts of lithologies from both upper and lower plates. (**d**) Thrust contact without fault gouge or sediment filling near Profile 5. (**e**) and (**f**) show thin-section images from the molasse and the Aztec Sandstone. Notice larger pores, red iron coatings, and larger and better sorted grains for the Aztec Sandstone.

Downloaded from http://sp.lyellcollection.org/ by guest on April 28, 2017

Downloaded from http://sp.lyellcollection.org/ by guest on April 28, 2017

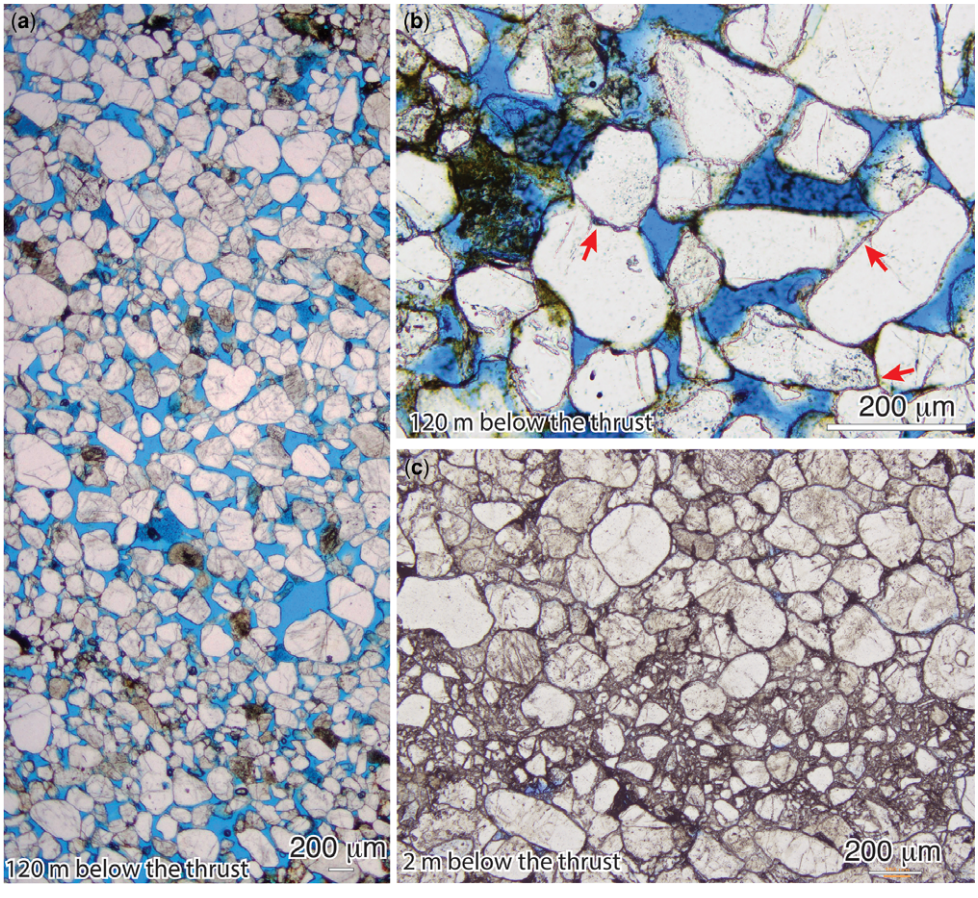

Fig. 4. Thin-section photographs of little-deformed Aztec Sandstone (**a**, **b**) with evidence of pressure solution (arrows). Deformed sandstone close to the thrust (**c**) shows little or no porosity, serrated grain boundaries indicative of pressure solution and a zone of grain crushing, and small, angular grain fragments.

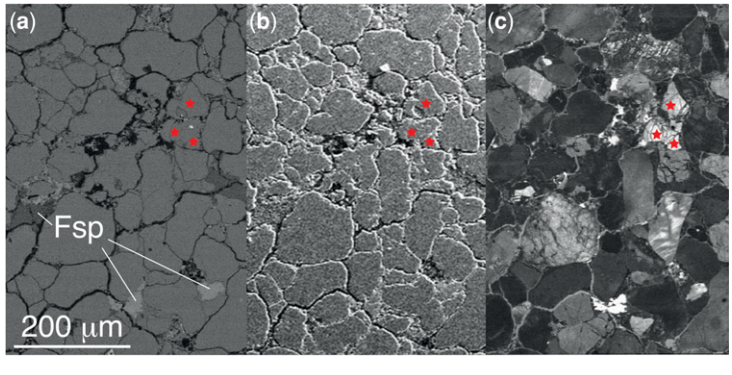

Fig. 5. SEM images of the Aztec Sandstone at 200×, 10 m below the thrust along Profile 1. (**a**) Backscatter image showing grain composition, with quartz being the most abundant followed by feldspars (Fsp) and secondary clay minerals (from X-ray spectrometry). (**b**) Secondary electron image. (**c**) Cathodoluminescence revealing fractures and healed cracks. Stars show an example of a grain in which cathodoluminescence reveal internal fractures that are otherwise difficult to discern.

Downloaded from http://sp.lyellcollection.org/ by guest on April 28, 2017

through the Aztec Sandstone, suggesting the presence of a ramp.

The fault gouge is up to 2 m thick, in which extreme cataclasis resulted in a fine-grained matrix of mostly crushed quartz grains overlain by a calcareous fault rock, with kinematic indicators suggesting extensional reactivation (Fig. 3b). This gouge sometimes mobilizes itself upwards into the fault breccias of the upper plate dolomites, characteristic of hydraulic brecciation. For a detailed characterization of the fault gouge, see Engelder (1974). The molasse interval, up to a few tens of metres thick, is restricted to the vicinities of profiles 1, 6 and 7, and exhibits mainly poorly sorted sandstones with calcareous cement (see Fig. 3e). Fluvial channels are metre-thick and contain conglomeratic clasts of carbonates and sandstones (Fig. 3c).

Away from the contact, intense cataclasis is replaced by localized deformation in the form of deformation bands (Fig. 2b, e); these modify the original grain arrangement of the sandstone, and therefore its petrophysical properties (see Fossen *et al.* 2015 for more details). Deformation bands are also observed close to the thrust, but are difficult to recognize due to the pervasive cataclasis at this structural level. As context for our analysis, a summary of their key observations is provided here as follows: deformation bands are subdivided into pure compaction bands (PCB; grain reorganization in the form of compaction and mild cataclasis); shear-enhanced compaction bands (SECB; grain reorganization in the form of compaction, mild cataclasis and minute shear only); and cataclastic shear bands (CSB; cataclasis and grain reorganization due to shearing and compaction). PCB display no shear offset while tabular and planar CSB and SECB accommodate shear offsets, the latter bands being significantly thicker and with significantly less shear offset (SECB are centimetre-thick whereas CSB show thicknesses of *c.* 1 mm; SECB offsets are difficult to see but are typically of a few millimetres; and CSB offsets reach up to few centimetres). In many cases CSB offset both SECB and PCB and, at the microscale, CSB involves significantly more grain comminution than the former two (see Fossen *et al.* 2015 for details).

Methods

Permeability profiles and sample collection

Ten transects were recorded from the thrust contact and downwards into the Aztec Sandstone to evaluate petrophysical variations of the sandstone in the footwall (Fig. 2b). Along these transects, a total of *c.* 130 permeability points were measured using a portable air permeameter (TinyPerm II by NER) from the thrust contact and downwards into the Aztec Sandstone after excavating fresh surfaces of host rock (Fig. 2b insets). Methodological details of this procedure are described in Filomena *et al.* (2014) and in Rotevatn *et al.* (2008). Permeability points were georeferenced by means of a handheld GPS device to record vertical (elevation) distances instead of outcrop/slope distances from the thrust contact. In addition, rock samples were collected along transects to study the micro-texture of the sandstone using polished thin-sections.

Converted TinyPerm II measurements tend to overestimate permeability by a factor of around 1.8 with respect to conventional Helium plug measurements in the Navajo and similar aeolian sandstones (Fossen *et al.* 2011), and the measurements presented here should be adjusted accordingly when comparing to such plug measurements. Uncertainties involved in measuring permeability with the TinyPerm permeameter are small, and were further reduced by performing repeated measurements at each point (Filomena *et al.* 2014). Furthermore, the overall trend of the transects (see below) and the consistency of typical values measured throughout the study area are consistent internally and with porosity estimates, and represent a sound basis for comparative analysis of permeabilities and permeability trends.

Porosity estimation using optical microscopy

Porosity of the Aztec Sandstone was estimated through areal quantification, calculating the percentage of blue-coloured epoxy (representing the pore fraction) in 50 thin-section photomicrographs acquired with conventional polarizing light microscopy. Deformation band porosity was also estimated where measurable porosity was visible in the photomicrographs. Image analysis was performed using ImageJ software (Rasband 1997–2014) to extract grain size and shape descriptors, as well as porosity using the Jpor plugin for ImageJ (Grove & Jerram 2011). Photo quality improvement was achieved in Adobe Photoshop. In addition, mercury injection porosimetry (Giesche 2006) was performed on three samples in the high-porosity domain far below the thrust contact, yielding a value (18.55%) comparable to those obtained from thin-section images from similar parts of the sandstone. All porosity measurements were plotted to compare and explore relationships with permeability points acquired in the field.

Electron microscopy (SEM-CL and SEM-BSE)

Twenty-three selected polished thin-sections were carbon coated and examined using a ZEISS Supra 55VP scanning electron microscope with a Centaurus Scintillator cathodoluminiscence detector

Downloaded from http://sp.lyellcollection.org/ by guest on April 28, 2017

(SEM-CL) in order to image textures at higher magnifications and constrain additional microstructural relationships (grain size and angularity) that would fall below the resolution of other techniques (Milliken & Laubach 2000; Milliken *et al.* 2005) (see Fig. 5). Nine of these thin-sections were then imaged using backscattering electrons (SEM-BSE) to extract shape descriptors (grain size and distribution, sorting and angularity) and constrain porosity measurements made with optical microscopy. Multi-point X-ray spectroscopy analysis was performed in all but two of those nine thin-sections in order to achieve information about composition of grains and surroundings.

Sections were placed at a working distance of 15 mm ($\pm$0.5) and 10 mm ($\pm$0.6) for SEM-CL and SEM-BSE, respectively, with an accelerating voltage of 15 kV and a probe current of *c.* 5 nA for both. Magnifications ranged mainly from 64× to 500×. Secondary electron images were examined simultaneously with both SEM-CL and SEM-BSE detectors to evaluate grain boundary morphologies and sample topography (see Fig. 5 for a comparison between the three techniques). For the microstructural description, we use the classification scheme for deformation mechanisms and microstructures proposed by Blenkinsop (2000).

Thrust-related deformation of the Aztec Sandstone

The mesoscopic thrust-related deformation of the Aztec Sandstone in the Buffington window is recognized by the presence of deformation band populations and more gradual variations in cohesion related to diffuse microscale deformation processes that also influence the petrophysical (porosity, permeability) properties of the sandstone. The microstructural aspects of this deformation are explored here, while the petrophysical effects are assessed in the following section.

Cataclasis

The microscale deformation of the Aztec Sandstone, as explored in thin-sections by means of the optical and electron microscope, can be classified as cataclasis (grain reorganization with various degrees of grain comminution), and diffusive mass-transfer dissolution (i.e. pressure solution). Cataclasis generally occurs: (1) pervasively near the thrust contact (Fig. 3c); (2) more diffuse at a distance from the thrust contact; and (3) localized within deformation bands throughout the sandstone. In addition, extreme cataclasis is expressed in the thrust fault gouge zone (Fig. 3b), which contains a mixture of brittle deformed material from the footwall (sandstone) and hanging wall (see Engelder 1974 for a detailed account of the Muddy Mountains thrust fault gouge).

In general, cataclasis is recognized from intragranular fractures, a high degree of grain angularity and significant grain size reduction as compared to the more intact Aztec Sandstone far away from the thrust. The difference between pristine sandstone and strongly affected sandstone is well exemplified by Figures 4 and 6d. Figure 6d, collected from the cataclastic and indurated zone below the thrust, shows a large variation in grain size and low porosity, and also intragranular fractures. A few intragraunlar fractures are also seen in Figure 6a, which was collected 79 m vertically below the thrust, suggesting that the sandstone did not escape deformation completely even at 50–100 m into the footwall. However, for the most part the grains are intact and rounded, and larger with a more even size than the deformed version shown in Figure 6d.

The set of grain size histograms shown in Figure 7 (from Profile 3) portray the overall decrease in grain size upwards towards the thrust. For the most distant sample at 108 m below the thrust (Fig. 7, bottom) the grain size averages 0.25 mm (fine-to-medium-sand size), while close to the thrust the grain size averages 0.07 mm (fine-to-medium-silt size) for the nearest sample closest to (at 7 m below) the thrust (Fig. 7, top). The sandstone near the thrust also shows a very large range in grain size, from clay-size up to medium-to-coarse sand (Fig. 7, top), while for the sample at 108 m all grains are sand-sized. It should be noted, however, that within the indurated zone there are bands of stronger grain-size reduction that may be explained as shear bands separating less sheared and crushed, but considerably indurated, domains of sandstone (Fig. 4c).

In terms of angularity, thin-section studies show that grains of the Aztec Sandstone generally become more angular towards the thrust contact (compare Fig. 6a, d). It is also clear that grains belonging to the smaller portion of the size population are more angular than the larger grains, which is a characteristic feature of grain comminution.

Grain comminution is also evident within deformation bands. This effect is very pronounced in cataclastic deformation bands, where grain size is reduced by at least one order of magnitude relative to the host rock (Fig. 7, CSB at 84 m from the thrust). The thicker shear-enhanced compaction bands (SECB) show a lower level of grain comminution (Fig. 7, at 61 m and 84 m from the thrust). The reason for this is probably the low strains (displacements) accumulated by the SECB. A similar low amount of comminution is also seen within pure compaction bands, which also involve very low strains. Similarly, high shear strains in the thin CSB produce angular and small grain fragments,

Downloaded from http://sp.lyellcollection.org/ by guest on April 28, 2017

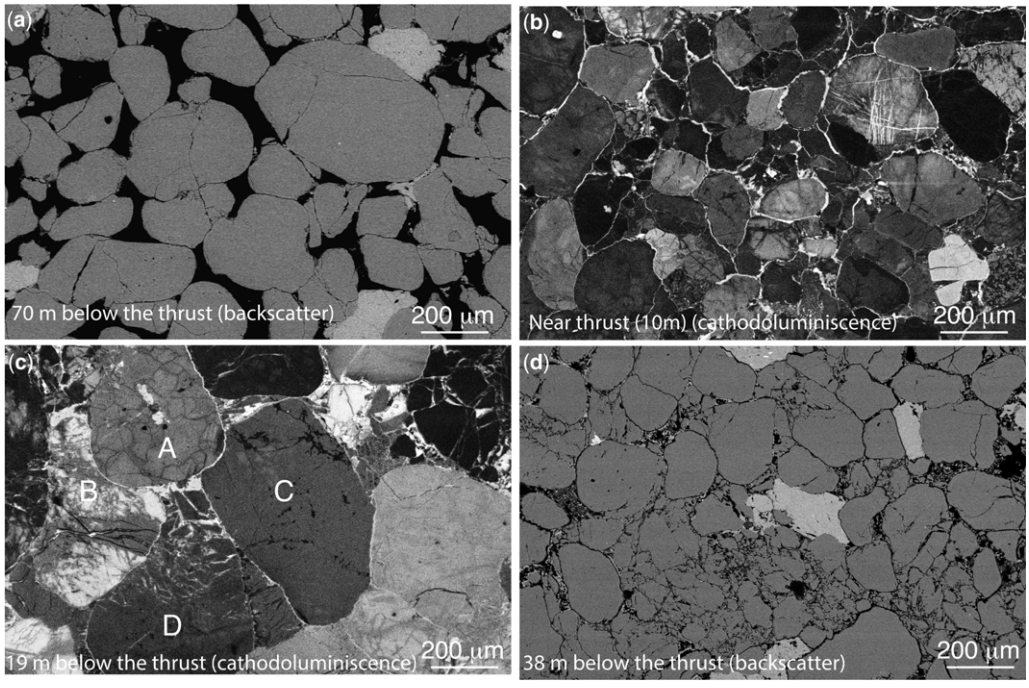

Fig. 6. SEM images of Aztec Sandstone microstructures. (**a**) Little-deformed sandstone 70 m below the thrust. The sandstone has *c.* 20% porosity and shows some intragranular fractures, but only very limited grain comminution. (**b**) Secondary electron image of the sandstone closer to the thrust, showing loss of porosity and serrated pressure-solution-style boundaries. (**c**) Deformed sandstone, showing evidence of pressure solution (e.g. grain A indenting into B and C) as well as grain comminution (e.g. B and D), indented pressure solution contacts in less-fractured grains (red stars). (**d**) Deformed sandstone showing variable amounts of grain-size reduction with the formation of small, angular clasts suggestive of grain comminution.

whereas grains inside SECB and PCB are only slightly more angular than the host rock (Fossen *et al.* 2015).

Diffusive mass transfer

Evidence for diffusive mass transfer can be found in any part of the sandstone in the form of indented and truncated grain boundaries (Fig. 6), also in relatively pristine sandstone such as those shown in Figures 4b and 6a. There is an overall increase in such evidence along with the general increase in cohesion of the sandstone towards the thrust (Fig. 6), although the intensity varies even at the outcrop scale. In contrast to the abundant evidence of pressure solution very limited amounts of precipitation (cement) have been identified, and mostly in the form of marginal overgrowths. Where the sandstone is highly indurated, particularly near the thrust contact, the cohesive nature of this part of the sandstone has resulted in networks of joints with the formation of diagenetic colouration patterns known as liesegang rings.

While pressure-solution is clearly important, closer examination under cathodoluminiscence reveals that many grains that show shapes and boundary geometries typical of dissolution also deform by pervasive internal grain fracturing (Figs 5c & 6c). This grain crushing is not equally evident in backscatter and secondary electron microscopy images (Fig. 5a, b). While pressure solution appears to be an important or even the dominant mechanism in several of the thin-sections investigated, the fact that pervasive grain fracturing may be hard to detect under the optical microscope can potentially lead to an overestimation of the effect of pressure solution. Clearly a combination of cataclasis and pressure solution is responsible for the observed increase in cohesion, loss of porosity and reduction in grain size towards the thrust and, while both are important, more work is needed to quantify their relative importance.

Within the cataclastic deformation bands (CDB), grain size reduction is mainly caused by grain fracturing, while diffusive mass-transfer adds to the cohesion of the bands. However, SECB and PCB show a more significant component of dissolution; again, the change in grain shape associated with some grain contacts can also be caused by dense

Downloaded from http://sp.lyellcollection.org/ by guest on April 28, 2017

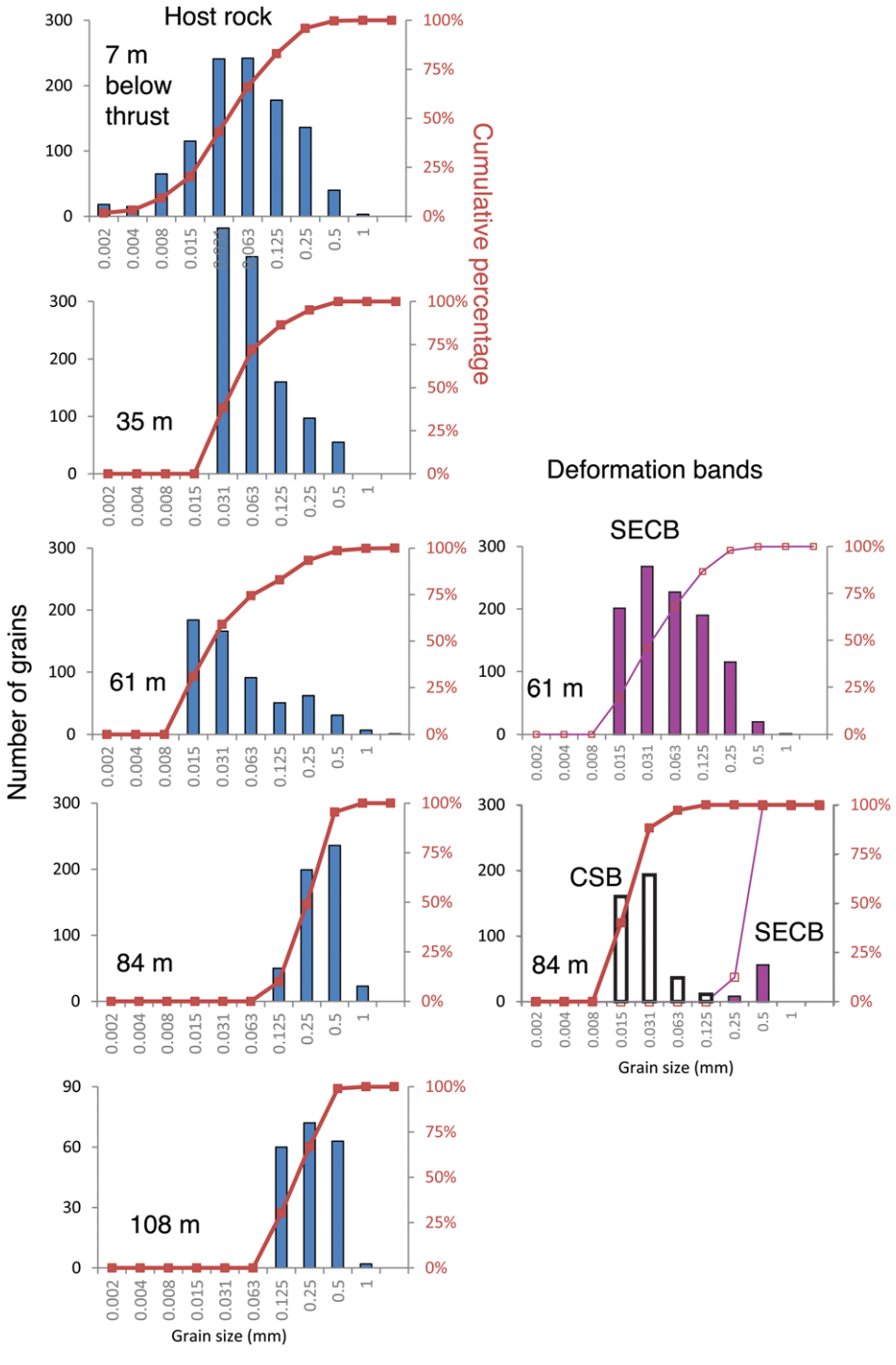

Fig. 7. Grain size distribution for host rock (left) and deformation band (right) samples in Profile 3, from 7 to 108 m below the thrust. Generally, grain sizes are finer closer to the thrust. Notice that for deformation bands, grain size reduction is important for cataclastic shear bands (CSB), while shear-enhanced compaction bands (SECB) maintain grain sizes more similar to the host rock.

Downloaded from http://sp.lyellcollection.org/ by guest on April 28, 2017

networks of microfractures, similar to that shown in Figure 6c.

Petrophysical effects of thrusting on the Aztec Sandstone

The results from the collected vertical permeability profiles are shown in Figure 8. The data show present-day permeabilities for the Aztec Sandstone in the Buffington window ranging over *c.* 10–4000 mD. The highest permeabilities are, as expected, found in the deepest parts of the sandstone, that is, far away from the thrust contact; there is also a clear trend of permeability increase downwards from the thrust fault, in some cases to more than 100 m below the thrust (Profiles 5 and 7 in Fig. 8). Qualitatively, this trend is consistently reflected by the ten profiles of Figure 8, although somewhat less clearly for Profile 1 which is of very limited vertical extent. Quantitatively, however, there is some variation in the steepness of the permeability trends. Profiles 2, 5 and 8 show that within *c.* 40–60 m vertically below the thrust, the sandstone permeability has increased one order of magnitude, eventually reaching maxima of 1–4 Darcy at the end of the profiles. Profiles 7 and 9, on the other hand, show a more gentle increase in permeability, with maximum values of *c.* 100–300 mD and continuous permeability increase all the way to >100 m vertically below the thrust contact.

Porosity measurements from thin-sections along the profiles are shown in Figure 9. Host rock porosities range from 20% to almost zero towards the thrust contact, whereas the sample analysed with mercury porosimetry resulted in a value of 18.6%. Maximum porosity values are higher in profiles from the eastern part of the Buffington window, namely profiles 2, 3, 5 and 10 (with the exception of Profile 4), whereas porosity values never exceed 15% in profiles from the western side (Profiles 6, 7, 8 and 9). The porosity profiles in Figure 9 contain measurements that appear more scattered than their permeability counterparts, but a general increase in porosity vertically downwards from the thrust and into the Aztec Sandstone is apparent. The porosity inside deformation bands (open data points in Fig. 9) also varies, partly as a function of deformation band type: cataclastic shear bands reveal significant reductions in porosity, while pure compaction and shear enhanced compaction bands retain porosities only slightly below those of their surrounding host rock (see diamonds v. squares in Fig. 9).

Porosity and permeability profiles exhibit the same overall trend: low porosities and permeabilities near the thrust contact, and increasing porosities and permeabilities at increasing vertical distance from the thrust contact and into the Aztec Sandstone. However, there are also differences that are worth noting. Profile 8, despite a downwards overall increasing trend for both porosity and permeability, displays relatively high overall permeability values, but comparatively low porosity values (Figs 8 & 9).

Discussion

Grain size distributions

Our results for grain size variations as a function of thrust distance are generally in accordance with those of Brock & Engelder (1977), with the exception of our incorporation of grain size reductions away from the thrust associated with deformation band cataclasis; as previously mentioned, these become significant for CSB (Fig. 7).

Figure 10 shows a comparison between Brock and Engelder's traverses and our own profiles (see stars in Fig. 2a). Brock and Engelder's western traverse lies in proximity to profiles 6 and 7, and their northern traverse with Profile 10. Their southern traverse was closest to Profile 5; however, according to recent geological maps of the area (Beard *et al.* 2007; Felger & Beard 2010), the contact between the Aztec Sandstone and the Bonanza King Formation in that area is defined by a normal fault and not by the Muddy Mountains thrust.

Profile 10 exhibits smaller grain sizes than Brock and Engelders' northern traverse (triangles in Fig. 10), but share the same stability of grain sizes with increasing distance from the thrust (grains are always fine-to-medium sand in Profile 10, and medium-to-coarse sand in their northern traverse). Profile 6 and Brock and Engelders' western traverse (squares in Fig. 10) are located in the part of the window containing the unnamed clastic interval between the plates. Resulting grain sizes show a close correspondence, including the increase in grain size once the clastic interval or 'molasse' finishes and the sandstone starts. The thickness of this interval is somewhat larger for our profile than theirs (47 v. 33 m). The first drop in all series represents the transition from the fine-grained cataclastic narrow zone at the thrust contact towards the less-affected Aztec Sandstone, whereas subsequent variations in the graph correspond to more local variations in the character and properties of the sandstone.

Deformation mechanisms, controls and timing

Figure 11 summarizes the types of deformation found in the Aztec Sandstone with respect to the geological history of the area, as well as the petrophysical effects associated with each deformation phase. According to the kinematic history proposed by Fossen *et al.* (2015) for the Sevier phase, PCB

Downloaded from http://sp.lyellcollection.org/ by guest on April 28, 2017

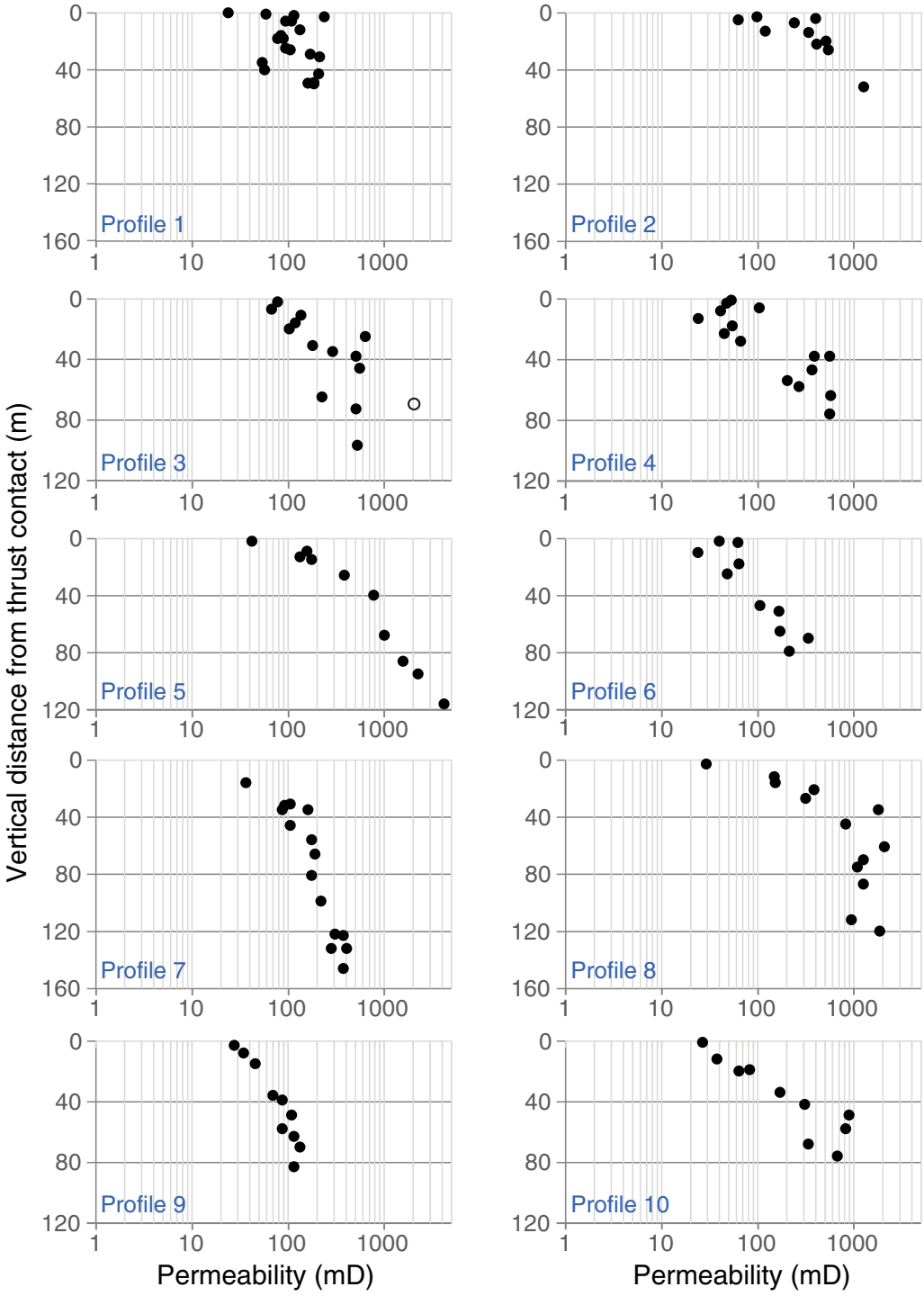

Fig. 8. Permeability profiles for the Aztec Sandstone at the Buffington window. Vertical axes represent distance (vertical) from the thrust contact; horizontal axes are permeability (K) in millidarcys. The result of a mercury injection porosimetry lab test of a sample from this profile is shown as an open circle.

Downloaded from http://sp.lyellcollection.org/ by guest on April 28, 2017

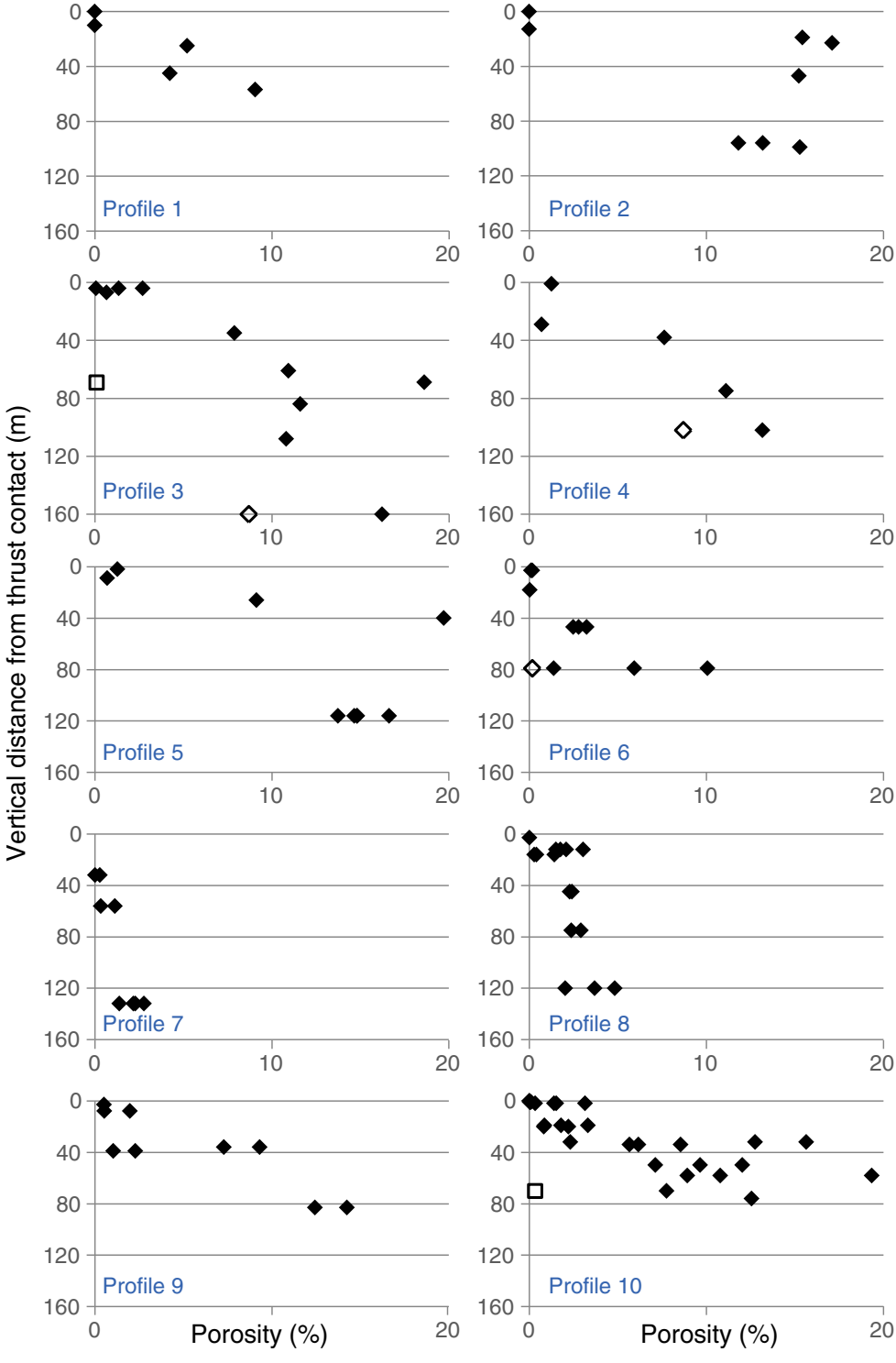

Fig. 9. Porosity profiles for the Aztec Sandstone at the Buffington window. Black diamonds are host-rock measurements, open symbols represent deformation band measurements (CSB squares, SECB diamonds).

Downloaded from http://sp.lyellcollection.org/ by guest on April 28, 2017

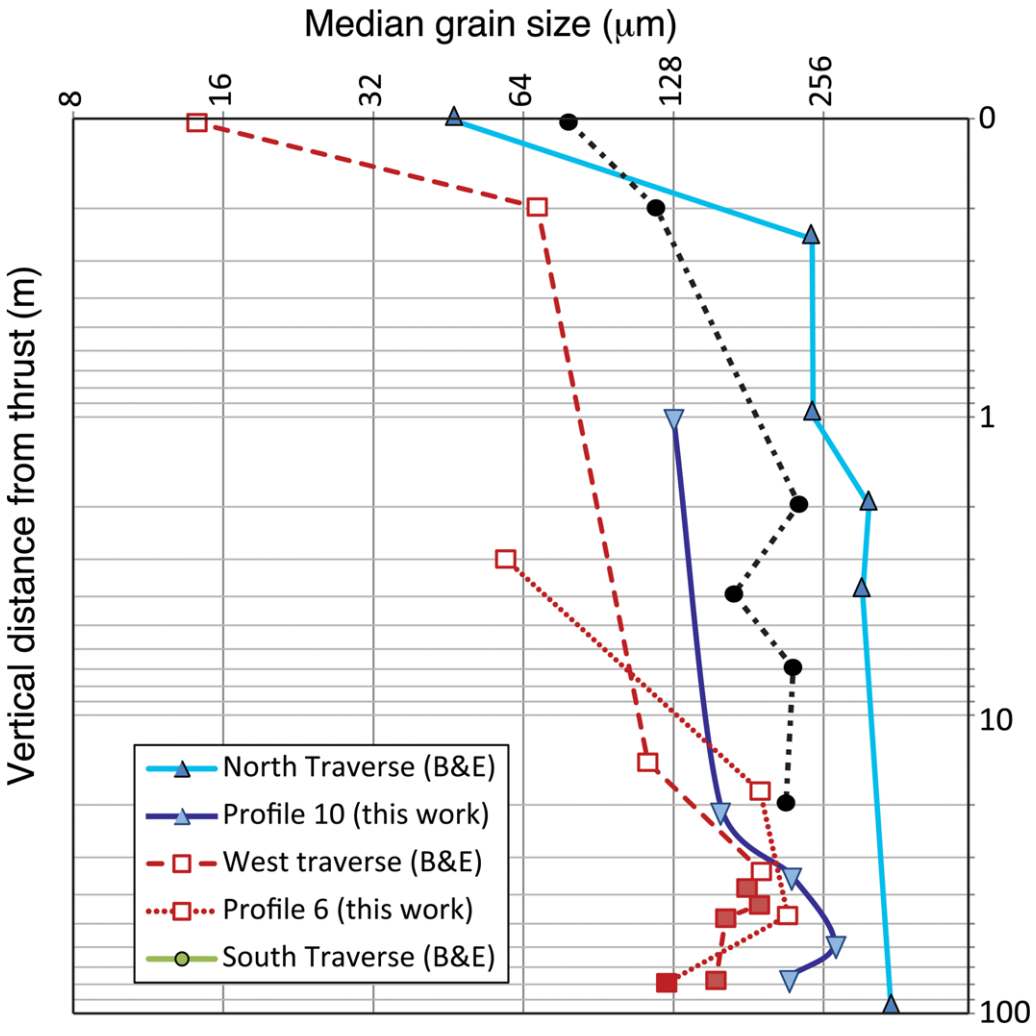

Fig. 10. Median grain size v. vertical distance from the Muddy Mountain thrust. Data from Brock & Engelder's (1977) northern and western traverses compared to profiles 10 and 6 of this study (see stars in Fig. 2a). Hollow markers in west traverse and Profile 6 correspond to samples from the 'molasse', while colour-filled markers belong to samples from the Aztec Sandstone.

and SECB formed at early stages of the shortening. Since PCB and SECB show little modification of grain framework with respect to the host rock, petrophysical properties were largely maintained.

As thrusting proceeded, mechanical compaction increased both vertically (due to the loading from the upper plate emplacement) and horizontally (as shortening continues). At some critical point during overall porosity reduction and stress build-up, a change from formation of SECB/PCB (Fig. 12a) to CSB (Fig. 12b) occurred. Simultaneously, the tectonic transport of the thrust caused cataclasis and indurated the Aztec Sandstone in a wide zone below the thrust contact.

The pressure solution that is seen in the indurated tight sandstone near the thrust is likely to have occurred at a late stage of thrusting and/or immediately after thrusting. In general, dissolution of quartz occurs efficiently only at temperatures $>80–90^{\circ}C$ because the kinetics of dissolution/precipitation are too slow at lower temperatures (e.g. Oelkers *et al.* 1996; Bjørkum *et al*. 1998). Such temperatures require significant ($\geq$3 km) burial, which was not achieved until advanced stages of thrusting.

While we can relate deformation band orientations and variations in cataclasis and induration directly to thrusting, joints and calcite-filled veins that consistently post-date deformation bands of

Downloaded from http://sp.lyellcollection.org/ by guest on April 28, 2017

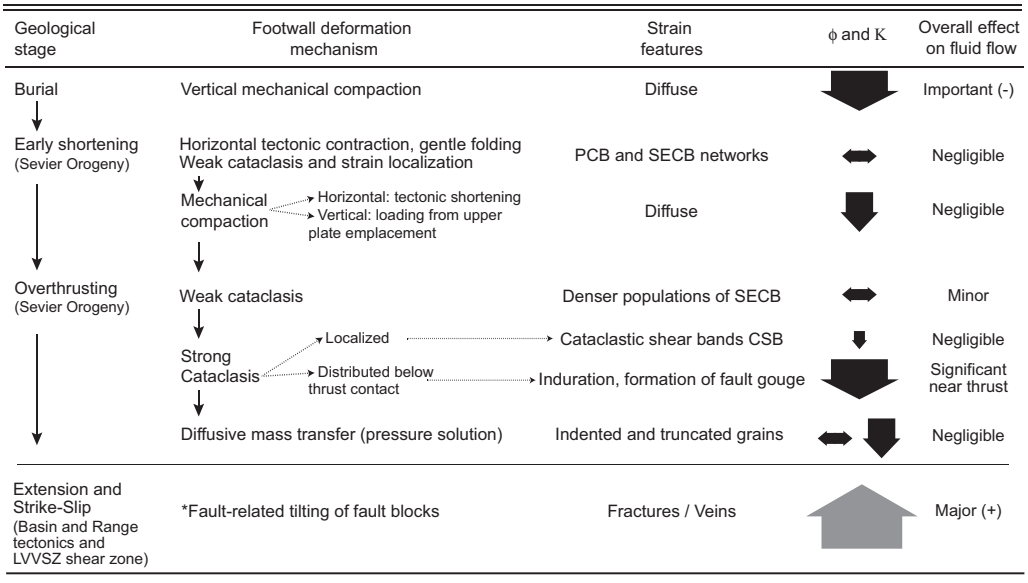

Fig. 11. Deformation mechanisms, associated strain features and effects on petrophysical properties related to each deformation phase affecting the Aztec Sandstone in the Buffington window, with main focus on the Sevier shortening phase. Arrows represent porosity/permeability decrease (downwards) and increase (upwards). Arrow thickness conveys the magnitude of alteration for the zones in which they occur. Overall effect refers to the entire sandstone body. Notice that for the overthrusting phase, although CSB and near-thrust induration reduce porosity (ϕ) and permeability (K) significantly, their thicknesses and spatial occurrences become less important at the scale of the entire outcrop. LVVSZ: Las Vegas Valley shear zone.

all kinds have orientations that conform with Basin and Range extension, consistent with interpretation from the nearby Valley of Fire area (Zhou *et al.* 2012). Furthermore, the thrust is offset by normal and strike-slip faults with hundreds of metres of displacement that, from regional considerations, are clearly of Basin and Range type (Fossen *et al.* 2015). From what we have observed, these faults did not develop deformation bands in the Aztec sandstone, probably because of the induration of the sandstone and the stress conditions during the Basin and Range-related exhumation. We therefore also suggest that, contrary to what was proposed by Brock & Engelder (1977), most of the joints and meso-scale fractures that occur preferentially in indurated sandstone did not form during thrusting of the Muddy Mountain thrust sheet, but rather are related to deformation and exhumation during Basin and Range extensional tectonics.

Porosity and permeability trends

The current porosity and permeability distribution for the Aztec Sandstone in the Buffington window is the result of the interplay between the early burial history and the subsequent tectonic and diagenetic events that took place in the area. The consistent decrease in porosity and permeability towards the thrust contact demonstrated above shows a close connection between the change in rock properties and overthrusting, mainly by means of cataclasis and dissolution.

In terms of the permeability reductions caused by deformation bands, SECBs are associated with a permeability reduction by up to three orders of magnitude; two orders are most common, as reported in Fossen *et al.* (2015) and by Eichhubl *et al.* (2010) and Sun *et al.* (2011) in the nearby Valley of Fire State Park. Cataclastic shear bands can involve three orders of magnitude permeability reduction due to their intense comminution of grains.

High densities of SECB and PCB correlate with profiles where the Aztec Sandstone and the Bonanza King Dolomites are in direct contact or only separated by thin gouge. In those areas, the sandstone rapidly transitions into a more porous and friable rock. In contrast, near the thickest intervals of molasse the Aztec Sandstone remains indurated over large vertical intervals (Profile 7 in Fig. 8). For these areas, PCB and SECB were not found. It could be argued that such forethrust debris caused additional vertical loading that resulted in compaction and porosity reduction of the sandstones at depth, preventing them from developing PCB and SECB. At present, more work is needed to explain

Downloaded from http://sp.lyellcollection.org/ by guest on April 28, 2017

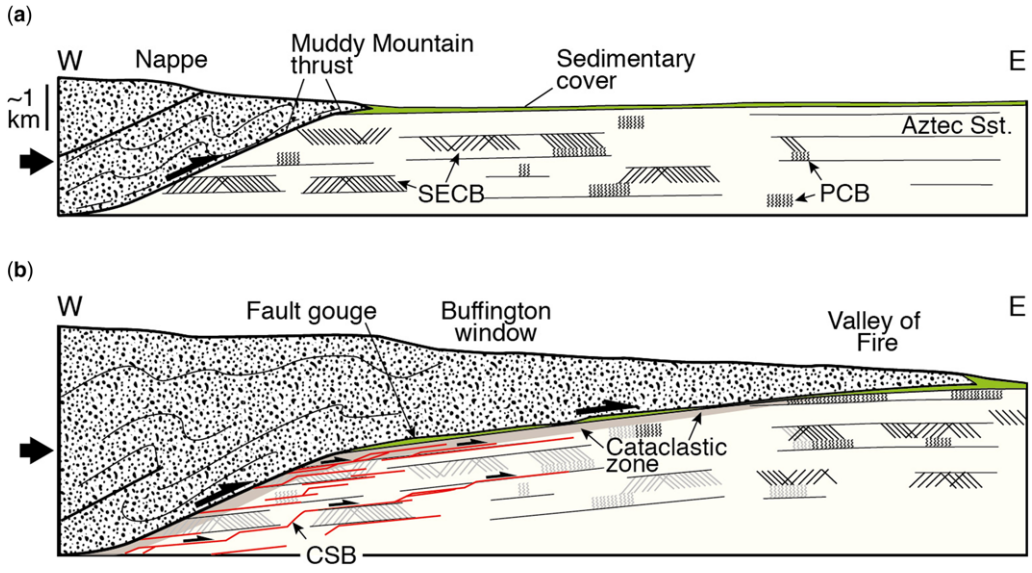

Fig. 12. Very schematic illustration of (**a**) early and (**b**) late stages of Sevier overthrusting in the study area, based on results from this work and Fossen *et al.* (2015). (a) SECB and PCB form at early stages of thrusting beneath and ahead of the thrust sheet. (b) CSB, many sub-parallel to bedding, form at greater burial depth, overprinting other SECB and CSB. Faulting and block rotation during the later Basin and Range extension is not shown.

the difference in character of the western v. eastern part of the Aztec Sandstone in the Buffington window (including estimations regarding heights and vertical loading of the original alluvial fan at the time of foreland basin infilling, and other diagenetical controls).

Reservoir implications

The findings of the present study in terms of petrophysical alterations within the sandstones in the footwall of the thrust have implications for fluid flow in similarly set reservoirs in the subsurface. Overall, the findings show a significant increase in permeability downwards from the thrust over a zone of the order of 100 m in thickness. This would translate into an upwards-deteriorating flow property trend towards the thrust. In particular, the low-permeable envelope along the thrust represents a zone of poor flow properties, although it does not reach permeabilities low enough to form a top seal.

Deformation deeper down into the sandstone is highly localized and appears in the form of deformation bands. Although these are associated with a reduction in permeability, other studies (e.g. Fossen & Bale 2007; Rotevatn & Fossen 2011) have shown that deformation bands must be of exceedingly low permeability and abundant to significantly affect flow in a negative way. What is likely, however, and also supported by the aforementioned studies, is that the deformation bands in the sandstones below the thrust would baffle and redirect flow, leading to a more tortuous flow pattern.

If we were to consider the sandstones in the Buffington window as a direct geological and geometrical reservoir-trap analogue, the porous parts of the sandstone would host fluids. The thrust contact, aided by the fault gouge zone, may potentially act as a seal. The thrust contact at the time of thrusting may have allowed the leakage of fluids but, after the gouge and induration resulting from the fault movement, an effective top seal can result from the low permeable zone in the sandstone near the thrust contact, making the configuration suitable for a post-thrusting hydrocarbon charging and entrapment. Additional compartmentalization effects caused by the deformation band networks are less likely due to the high porosity and permeability of the SECB and PCB and the relatively few and thin CSB, except for the case of very low fluid pressure gradients. Note that jointing associated with the late extensional phase as well as with uplift could compromise seal properties and/or encourage migration through the secondary porosity of the fractures.

How different is the contractional regime?

The contractional regime is different from the extensional regime when it comes to the type of structures formed, their distribution within deformed

Downloaded from http://sp.lyellcollection.org/ by guest on April 28, 2017

sandstones, and the existence of a roof thrust with associated cataclastic deformation along and beneath the thrust. Three types of deformation bands have been described in the porous sandstones underneath the Muddy Mountain thrust: pure compaction bands; shear-enhanced compaction bands; and cataclastic shear bands. Only shear bands have been described from the extensional regime and, depending on the degree of cataclasis involved, may reduce fluid flow if they occur in large numbers as clusters (Ballas *et al.* 2015). However, SECB and PCB have less of an effect on permeability and fluid flow (Fossen *et al.* 2015). CSB, which may have more of a permeability-reducing effect, tend to be low angle where related to thrust tectonics, and mostly add to the anisotropy already defined by the stratigraphy.

As discussed in more detail by Soliva *et al.* (2016), the strong clustering of deformation bands that characterizes the extensional (normal fault) regime is not very apparent in the contractional regime. Instead, the bands are more widely distributed, and form preferentially in highly porous parts of the reservoir. This means that they may homogenize the fluid flow pattern in a reservoir and reduce the chance for early water break-through by slowing down the flow in highly permeable sandstone layers. The *c.* 100 m thick damage zone to the thrust will, as discussed above, represent a major low-angle element of reduced flow that is different in terms of orientation and size from any structure expected to form in the extensional regime. This will also be the main element of concern during production in an overthrust reservoir of the kind described from the Buffington window.

Conclusions

- The movement and emplacement of the Sevier-age Muddy Mountain thrust nappe over the Aztec Sandstone in SE Nevada had the following structural impacts on the porous sandstone: (1) early formation of networks of shear-enhanced compaction bands during early shortening; (2) a gradual increase in distributed grain communition and pressure solution over an up to 150 m thick zone underneath the thrust; with (3) an intense cataclastic zone immediately underneath the thrust.
- Petrophysical effects of this deformation are significant permeability and porosity loss in a zone some tens of metres thick below the thrust plane, whereas porosity and permeability increases away from the thrust contact.
- The main porosity and permeability reduction mechanisms are cataclasis and pressure solution, while cementation is negligible.
- The lack of significant cementation supports the evidence for an open thrust system, with local or episodic fluid entrapment.
- The 'molasse' and channels that locally overlay the Aztec Sandstone correlate with a more gradual increase in permeability and porosity for the profiles nearby (higher induration). At present the specifics of this correlation are not constrained, so is not possible to establish the actual controls for this correlation.
- Deformation due to long-distance overthrusting above highly porous sandstones has localized effects that adversely affect petrophysical properties. Although this may locally lead to baffling and redirection of flow, a significant reduction of effective reservoir properties is only to be expected in a decametre-wide zone close to the thrust.

This work is part of the Contraction of Porous Sandstones project (COPS), hosted at the Centre for Integrated Petroleum Research (Uni Research CIPR) and the Department of Earth Science at the University of Bergen (UiB). Statoil is gratefully acknowledged for funding fieldwork. Constructive comments by Jennie Cook and an anonymous reviewer are highly appreciated, as are comments by Eric Flodin, Atilla Aydin and Peter Eichhubl on earlier versions of the manuscript.

References

Aydin, A. & Johnson, A.M. 1983. Analysis of faulting in porous sandstones. *Journal of Structural Geology*, **5**, 19–31.

Ballas, G., Fossen, H. & Soliva, R. 2015. Factors controlling permeability of cataclastic deformation bands and faults in porous sandstone reservoirs. *Journal of Structural Geology*, **76**, 1–21.

Beard, L., Anderson, R. *et al.* 2007. *Preliminary Geologic Map of the Lake Mead 30' × 60' Quadrangle, Clark County, Nevada, and Mohave County*. US Geological Survey, Arizona.

Bjørkum, P.A., Oelkers, E.H., Nadeau, P.H., Walderhaug, O. & Murphy, W.M. 1998. Porosity prediction in quartzose sandstones as a function of time, temperature, depth, stylolite frequency, and hydrocarbon saturation. *American Association of Petroleum Geologists Bulletin*, **82**, 637–648.

Blakey, R.C., Peterson, F. & Kocurek, G. 1988. Synthesis of late Paleozoic and Mesozoic eolian deposits of the Western Interior of the United States. *Sedimentary Geology*, **56**, 3–125.

Blenkinsop, T. 2000. *Recognition of Deformation, Microstructures and Mechanisms in Rocks*. Chapman & Hall/CRC Press, New York, USA.

Bohannon, R.G. 1983. Geologic map, tectonic map, and structure sections of the Muddy and northern Black Mountains, Clark County, Nevada. US Geological Survey, scale 1:62500.

Brandenburg, J.P., Alpak, F.O., Solum, J.G. & Naruk, S.J. 2012. A kinematic trishear model to predict

Downloaded from http://sp.lyellcollection.org/ by guest on April 28, 2017

deformation bands in a fault-propagation fold, East Kaibab monocline, Utah. *American Association of Petroleum Geologists Bulletin*, **96**, 109–132.

Brock, W.G. & Engelder, J.T. 1977. Deformation associated with the movement of the Muddy Mountain overthrust in the Buffington window, southeastern Nevada. *Geological Society of America Bulletin*, **88**, 1667–1677.

Carpenter, D.G. & Carpenter, J.A. 1994. Fold-thrust structure, synorogenic rocks, and structural analysis of the North Muddy and Muddy Mountains, Clark County, Nevada. *In*: *Proceedings Structural and Stratigraphic Investigations and Petroleum Potential of Nevada, with Special Emphasis South of the Railroad Valley Producing Trend. Nevada Petroleum Society Conference*, Reno, Nevada, **2**, 65–94.

Carr, M.D. 1980. Upper Jurassic to Lower Cretaceous(?) synorogenic sedimentary rocks in the southern Spring Mountains, Nevada. *Geology*, **8**, 385–389.

DeCelles, P.G. & Coogan, J.C. 2006. Regional structure and kinematic history of the Sevier fold-and-thrust belt, central Utah. *Geological Society of America Bulletin*, **118**, 841–864.

Eichhubl, P., Hooker, J.N. & Laubach, S.E. 2010. Pure and shear-enhanced compaction bands in Aztec Sandstone. *Journal of Structural Geology*, **32**, 1873–1886.

Engelder, J.T. 1974. Cataclasis and the generation of fault gouge. *Geological Society of America Bulletin*, **85**, 1515–1522.

Felger, T.J. & Beard, L.S. 2010. Geologic map of Lake Mead and surrounding regions, southern Nevada, southwestern Utah, and northwestern Arizona. *Geological Society of America Special Papers*, **463**, 29–38.

Filomena, C., Hornung, J. & Stollhofen, H. 2014. Assessing accuracy of gas-driven permeability measurements: a comparative study of diverse Hassler-cell and probe permeameter devices. *Solid Earth*, **5**, 1–11.

Fossen, H. & Bale, A. 2007. Deformation bands and their influence on fluid flow. *American Association of Petroleum Geologists Bulletin*, **91**, 1685–1700.

Fossen, H., Schultz, R.A. & Torabi, A. 2011. Conditions & implications for compaction band formation in the Navajo Sandstone, Utah. *Journal of Structural Geology*, **33**, 14.

Fossen, H., Zuluaga, L.F., Ballas, G., Soliva, R. & Rotevatn, A. 2015. Contractional deformation of porous sandstone. Insights from the Aztec Sandstone, SE Nevada, USA. *Journal of Structural Geology*, **74**, 172–184.

Giesche, H. 2006. Mercury porosimetry: a general (practical) overview. *Particle & Particle Systems Characterization*, **23**, 9–19.

Grove, C. & Jerram, D.A. 2011. jPOR: an ImageJ macro to quantify total optical porosity from blue-stained thin sections. *Computers & Geosciences*, **37**, 1850–1859.

Johnson, M. 1981. The erosion factor in the emplacement of the Keystone thrust sheet (South East Nevada) across a land surface. *Geological Magazine*, **118**, 501–507.

Langenheim, V.E., Grow, J.A., Jachens, R.C., Dixon, G.L. & Miller, J.J. 2001. Geophysical constraints on the location and geometry of the Las Vegas Valley Shear Zone, Nevada. *Tectonics*, **20**, 189–209.

Longwell, C.R. 1922. The Muddy Mountain overthrust in southeastern Nevada. *Journal of Geology*, **30**, 63–72.

Longwell, C.R., Pampeyan, E. & Bowyer, B.R. 1965. Geology and mineral deposits of Clark County, Nevada. *Nevada Bureau of Mines Bulletin*, **62**, 218.

Marzolf, J.E. 1990. Chapter 23: Reconstruction of extensionally dismembered early Mesozoic sedimentary basins; Southwestern Colorado Plateau to the eastern Mojave Desert. *Geological Society of America Memoirs*, **176**, 477–500.

Milliken, K.L. & Laubach, S.E. 2000. Brittle deformation in sandstone diagenesis as revealed by scanned cathodoluminescence imaging with application to characterization of fractured reservoirs. *In*: Pagel, M., Barbin, V., Blanc, P. & Ohnenstetter, D. (eds) *Cathodoluminescence in Geosciences*. Springer, Berlin Heidelberg, 225–243.

Milliken, K.L., Reed, R.M. & Laubach, S.E. 2005. Quantifying compaction and cementation in deformation bands in porous sandstones. *American Association of Petroleum Geologists Memoir*, **85**, 237–249.

Montañez, I.P. & Osleger, D.A. 1996. Contrasting sequence boundary zones developed within cyclic carbonates of the Bonanza King Formation, Middle to Late Cambrian, southern Great Basin. *Geological Society of America Special Paper*, **306**, 7–22.

Oelkers, E.H., Bjørkum, P.A. & Murphy, W.M. 1996. A petrographic and computational investigation of quartz cementation and porosity reduction in North Sea sandstones. *American Journal of Science*, **296**, 420–452.

Price, N.J. & Johnson, M.R.W. 1982. A mechanical analysis of the Keystone-Muddy Mountain thrust sheet in Southeast Nevada. *Tectonophysics*, **84**, 131–150.

Rasband, W. 1997–2014. ImageJ, US National Institutes of Health. Bethesda, Maryland, USA, v. 2012.

Rotevatn, A. & Fossen, H. 2011. Simulating the effect of subseismic fault tails and process zones in a siliciclastic reservoir analogue: Implications for aquifer support and trap definition. *Marine and Petroleum Geology*, **28**, 1648–1662.

Rotevatn, A., Torabi, A., Fossen, H. & Braathen, A. 2008. Slipped deformation bands: A new type of cataclastic deformation bands in Western Sinai, Suez rift, Egypt. *Journal of Structural Geology*, **30**, 1317–1331.

Schueller, S., Braathen, A., Fossen, H. & Tveranger, J. 2013. Spatial distribution of deformation bands in damage zones of extensional faults in porous sandstones: statistical analysis of field data. *Journal of Structural Geology*, **52**, 148–162.

Shipton, Z.K. & Cowie, P. 2001. Damage zone and slip-surface evolution over mm to km scales in high-porosity Navajo sandstone, Utah. *Journal of Structural Geology*, **23**, 1825–1844.

Soliva, R., Ballas, G., Fossen, H. & Philit, S. 2016. Tectonic regime controls clustering of deformation bands in porous sandstone. *Geology*, **44**, 423–426.

Sun, W., Andrade, J.E., Rudnicki, J.W. & Eichhubl, P. 2011. Connecting microstructural attributes and permeability from 3D tomographic images of in situ shear-enhanced compaction bands using multiscale computations. *Geophysical Research Letters*, **38**, https://doi.org/10.1029/2011GL047683.

Downloaded from http://sp.lyellcollection.org/ by guest on April 28, 2017

WERNICKE, B., AXEN, G.J. & SNOW, J.K. 1988. Basin and Range extensional tectonics at the latitude of Las Vegas, Nevada. *Geological Society of America Bulletin*, **100**, 1738–1757.

WILLEMIN, J.H. 1984. Erosion and the mechanics of shallow foreland thrusts. *Journal of Structural Geology*, **6**, 425–432.

ZHOU, X., KARIMI-FARD, M., DURLOFSKY, L.J. & AYDIN, A. 2012. Fluid flow through porous sandstone with overprinting and intersecting geological structures of various types. *In*: SPENCE, G.H., REDFERN, J., AGUILERA, R., BEVAN, T.G., COSGROVE, J.W., COUPLES, G.D. & DANIAL, J.-M. (eds) *Advances in the Study of Fractured Reservoirs*. Geological Society, London, Special Publications, **374**, 187–209.

ZULUAGA, L.F., FOSSEN, H. & ROTEVATN, A. 2014. Progressive evolution of deformation band populations during Laramide fault-propagation folding. Navajo Sandstone, San Rafael monocline, Utah, U.S.A. *Journal of Structural Geology*, **68**, 66–81.